

Nucleosynthesis in Massive Stars Including All Stable Isotopes

A. Heger¹, R. D. Hoffman², T. Rauscher^{1,3}, & S. E. Woosley¹

¹ *Astronomy Department,*

University of California, Santa Cruz, CA 95064, U.S.A.

² *Nuclear Theory and Modeling Group, L-414,*

Lawrence Livermore National Lab, Livermore, CA 94551-9900, U.S.A.

³ *Departement für Physik und Astronomie,*

Universität Basel, CH-4056 Basel, Switzerland

Abstract

We present the first calculations to follow the evolution of all stable isotopes (and their abundant radioactive progenitors) in a finely zoned stellar model computed from the onset of central hydrogen burning through explosion as a Type II supernova. The calculations were performed for a $15 M_{\odot}$ Pop I star using the most recently available set of experimental and theoretical nuclear data, revised opacity tables, and taking into account mass loss due to stellar winds. We find the approximately solar production of proton-rich isotopes above a mass number of $A = 120$ due to the γ -process. We also find a weak s-process, which along with the γ -process and explosive helium and carbon burning, produces nearly solar abundances of almost all nuclei from $A = 60$ to 85. A few modifications of the abundances of heavy nuclei above mass 90 by the s-process are also noted and discussed. New weak rates lead to significant alteration of the properties of the presupernova core.

1.1 Introduction

Stars above $\sim 10 M_{\odot}$ are responsible for producing most of the oxygen and heavier elements found in nature. Numerous studies of such stars and their detailed nucleosynthetic yields for various masses and metallicities, have been carried out previously, e.g., [32, 27]. However, our knowledge of both the input data and the physical processes affecting the evolution of these stars has improved dramatically in recent years. Updated opacity tables [12] have become available along with more accurate prescriptions for mass loss due to winds and new weak rates [16] that affect the evolutionary stages after central oxygen depletion. Perhaps most important for nucleosynthesis, new, accurate reaction rates for all the relevant strong and electromagnetic nuclear reactions above neon have been recently calculated by Rauscher and Thielemann [21]. Here we present the first results for a $15 M_{\odot}$ supernova evolved with the new physics. Additional masses and metallicities will be explored in future papers. These future papers will also include rotationally induced mixing processes [9].

We also employ a nuclear reaction network of unprecedented size. The nuclear reaction network used by [32] (WW95), large in its day, was limited to 200 isotopes and extended only to germanium (see also Chieffi and Limongi in these proceedings). Studies using nuclear reaction networks of over 5000 isotopes have been carried out for single zones or regions of stars, especially to obtain the r-process, e.g., [4, 5, 15], but “kilo-isotope” studies of nucleosynthesis in complete stellar models (typically of 1000 zones each) have been hitherto

lacking. We thus also present the first calculation to determine, self-consistently, the complete synthesis of all stable isotopes in any model for a massive star. However, because its thermodynamic properties continue to be poorly determined (and for lack of space), we will ignore here the nucleosynthesis that occurs in the neutrino wind, which may be the principal site of the r-process [31].

1.2 Input Physics

Our calculations were performed using a modified version of the stellar evolution code KEPLER [33, 32] with the following modifications:

- updated neutrino loss rates [13]
- improved opacity tables (OPAL95) [12, 29]
- mass loss due to stellar wind [19]
- updated weak rates [16]
- updated strong and electromagnetic reaction rates [21]

As in WW95, nucleosynthesis was followed by co-processing the stellar model throughout its evolution using an extended nuclear reaction network. From hydrogen ignition through central helium depletion a 617 isotope network was employed that included all elements up to polonium, adequate to follow the s-process. Just prior to central carbon ignition, we switched to a 1482 isotope network (also including astatine). This new network incorporated more neutron-rich isotopes to follow the high neutron fluxes in carbon (shell) burning. Five to ten isotopes were also added on the proton-rich side, in particular for the heavy elements, to follow the γ -process [30, 23, 24]. The nucleosynthesis during the supernova explosion itself was followed in each zone using a 2439 isotope network that included additional proton-rich isotopes to follow better the γ -process in the neon-oxygen core, and also many additional neutron-rich isotopes to follow the n-process expected during supernova shock front passage through the helium shell [3].

We implemented a new library of experimental and theoretical reaction rates. In particular, we used theoretical strong rates from [21] (using input from the FRDM [17]), experimental neutron capture rates (30 keV Maxwellian average) along the line of stability by [1], and experimental and theoretical rates for elements below neon as described in [11]. Experimental (α, γ) rates were implemented for ^{70}Ge [6] and ^{144}Sm [25]. The derived $\alpha + ^{70}\text{Ge}$ and $\alpha + ^{144}\text{Sm}$ potentials were also utilized to recalculate the transfer reactions involving these potentials.

Experimental β^- , β^+ , and α -decay rates were taken from [20], experimental β^- rates from [14] and [26], and theoretical β^- and β^+ rates from [18]. As a special case, we implemented the temperature-dependent ^{180}Ta decay as described in [2].

The supernova explosion was simulated, as in [32], by a piston that first moved inward for 0.45 s down to a radius of 500 km and then moved outward to a radius of 10 000 km such that a total kinetic energy of the ejecta at infinity of $1.2 \cdot 10^{51}$ erg resulted (for the $25 M_{\odot}$ stars we used a total kinetic energy of $1.5 \cdot 10^{51}$ erg). The final mass cut outside the piston was determined by the mass that had settled on the piston at $2.5 \cdot 10^4$ s after core collapse. Note that the amount of fallback resulting from this prescription depends on both the initial location of the piston used and the energy of the explosion. In particular, the yields of ^{44}Ti and ^{56}Ni are

very sensitive to this “final mass cut” determined by the fall back. Multidimensional effects of the explosion are not considered here. The temperature of the μ and τ neutrinos emanating from the proto-neutron star and causing the ν -process nucleosynthesis [34] were assumed to be 6 MeV in contrast to WW95 who assumed 8 MeV. However, we do not follow the ν -process for isotopes with Z or N larger than 40.

1.3 Results and Discussion

1.3.1 Stellar Structure

Table 1 gives the presupernova properties of our new models and, for comparison, those of WW95. The helium, carbon-oxygen, and neon-oxygen cores were defined as the location where hydrogen, helium, and carbon, respectively, first drop below a mass fraction of 1%, from the stellar surface going inward. The silicon core was defined by where silicon becomes more abundant than oxygen and the iron (“Fe”) core by where the sum of the mass fractions of ^{48}Ca and heavier nuclei first exceeds 50%. The deleptonized core was defined as the region where the number of electrons per baryon, Y_e , first drops below 0.49.

The lower helium core masses in the new models (Table 1) are due to both mass loss and the use of the OPAL opacities. In the $25 M_\odot$ case a model using OPAL opacities but no mass loss resulted in a helium core of $8.69 M_\odot$. As a result of the reduced helium core size our new models typically have lower helium-free and carbon-free cores. Due to the interaction of the

Table 1: Properties of stellar models at the onset of core collapse (*first section*) and integrated stellar yields of some important radioactive nuclei (*second section*).

		this work			WW95 [32]		
initial mass	(10^{34} g)	3	4	5	3	4	5
	(M_\odot)	15.08	20.11	25.14	15.08	20.11	25.14
final mass	(M_\odot)	12.64	14.23	13.87	15.08	20.11	25.14
He core	(M_\odot)	4.16	6.20	8.19	4.36	6.67	9.13
C/O core	(M_\odot)	2.82	4.57	6.38	2.47	4.37	6.54
Ne/O core	(M_\odot)	1.87	2.27	2.77	1.81	2.44	2.81
Si core	(M_\odot)	1.75	2.07	2.11	1.77	2.02	2.06
“Fe” core	(M_\odot)	1.55	1.47	1.74	1.32	1.74	1.78
delept. core	(M_\odot)	1.29	1.47	1.59	1.29	1.74	1.78
central Y_e		0.436	0.439	0.444	0.422	0.430	0.430
Pist. location	(M_\odot)	1.29	1.47	1.74	1.29	1.74	1.78
remnant mass	(M_\odot)	1.72	1.76	2.31 ^a	1.43	2.06	2.41 ^b
radioactive yields							
^{26}Al	(M_\odot)	$4.66 \cdot 10^{-5}$	$4.89 \cdot 10^{-5}$	$1.45 \cdot 10^{-4}$	$4.30 \cdot 10^{-5}$	$3.47 \cdot 10^{-5}$	$1.27 \cdot 10^{-4}$
^{44}Ti	(M_\odot)	$1.75 \cdot 10^{-5}$	$8.89 \cdot 10^{-6}$	$2.75 \cdot 10^{-6}$	$5.68 \cdot 10^{-5}$	$1.38 \cdot 10^{-5}$	$1.95 \cdot 10^{-6}$
^{56}Ni	(M_\odot)	$9.08 \cdot 10^{-2}$	$7.67 \cdot 10^{-2}$	$5.07 \cdot 10^{-3}$	$1.15 \cdot 10^{-1}$	$8.80 \cdot 10^{-2}$	$7.26 \cdot 10^{-5}$
^{60}Fe	(M_\odot)	$7.16 \cdot 10^{-5}$	$2.84 \cdot 10^{-5}$	$1.45 \cdot 10^{-4}$	$2.66 \cdot 10^{-5}$	$1.12 \cdot 10^{-5}$	$2.10 \cdot 10^{-5}$

^a $1.5 \cdot 10^{51}$ erg explosion

^b in [32] a remnant mass of $2.07 M_\odot$ is given in error for the $1.2 \cdot 10^{51}$ erg explosion. This change decreases significantly the yields of ^{56}Ni and ^{44}Ti (WW95: $1.29 \cdot 10^{-1} M_\odot$ and $3.04 \cdot 10^{-5} M_\odot$, respectively).

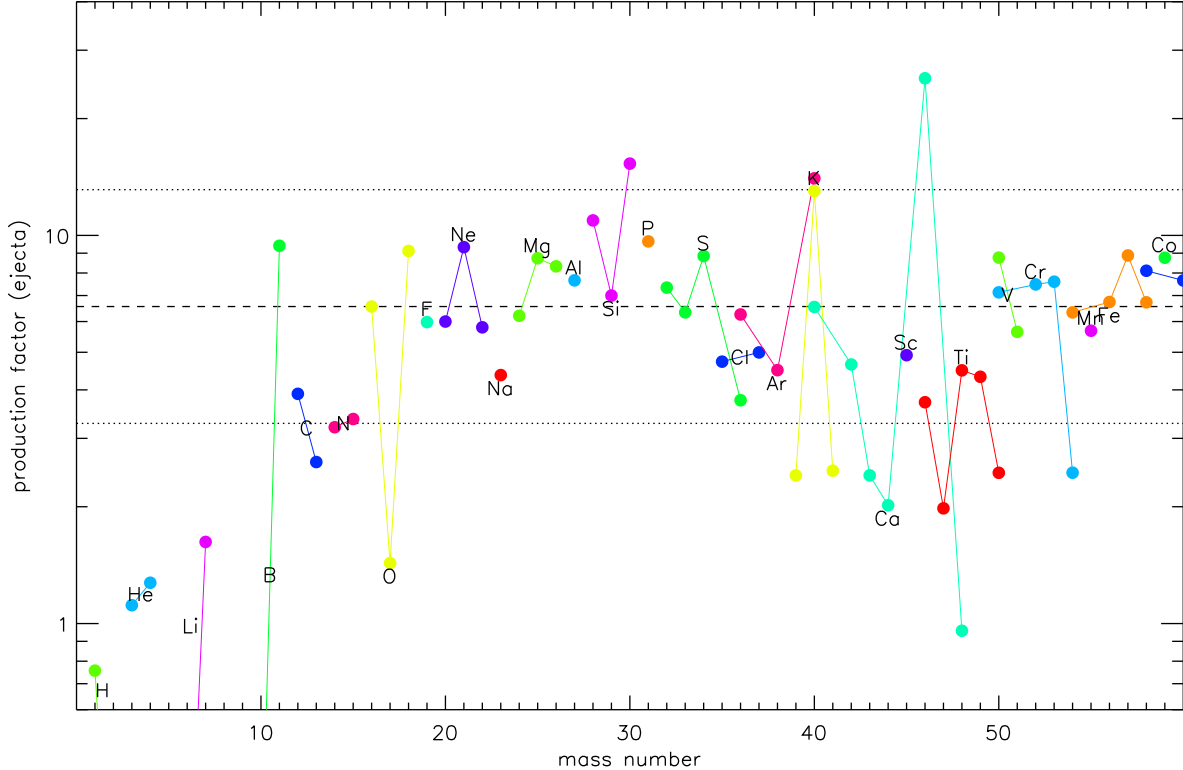


Figure 1: Production factors of iron group and lighter nuclei in a $15 M_{\odot}$ star of solar metallicity. Shown here are the average integrated abundances in the ejecta (including mass loss by stellar winds) relative to solar [7] (production factors). The *dashed line* indicates the production factor of ^{16}O and the *dotted lines* span a band of ± 0.3 dex.

different phases of shells burning, the sizes of the “inner cores” do not always monotonically change with the size of the helium core. More details will be given elsewhere [22, 9].

Some important changes in the new models are due to the revised weak rates [16]. These rates become important during core silicon burning and thereafter. Typically, they lead to an increase of the central Y_e at the onset of core collapse by 2 to 3% (Table 1), and this difference tends to increase with increasing stellar mass [8]. Perhaps more important for the explosion mechanism of core collapse supernovae is an increase of the density in the mass range of $m = 1.5 M_{\odot}$ to $2 M_{\odot}$ by 30 – 50% relative to the same models computed with the previous set of weak rates [32]. This may significantly affect the dynamics of the core collapse. For further details see [8].

1.3.2 Nucleosynthetic Production Factors

In Figs. 1 through 4 we show the production factors of all ejecta of the star after the explosion, including all the mass lost due to stellar winds, relative to solar [7] abundances. We assume that all radioactive nuclei have decayed to their stable products. As a gauge we provide the production factor of ^{16}O , the dominant “metal” produced in massive stars (*dashed line*), and a band of acceptable agreement of ± 0.3 dex relative to this values (*dotted lines*).

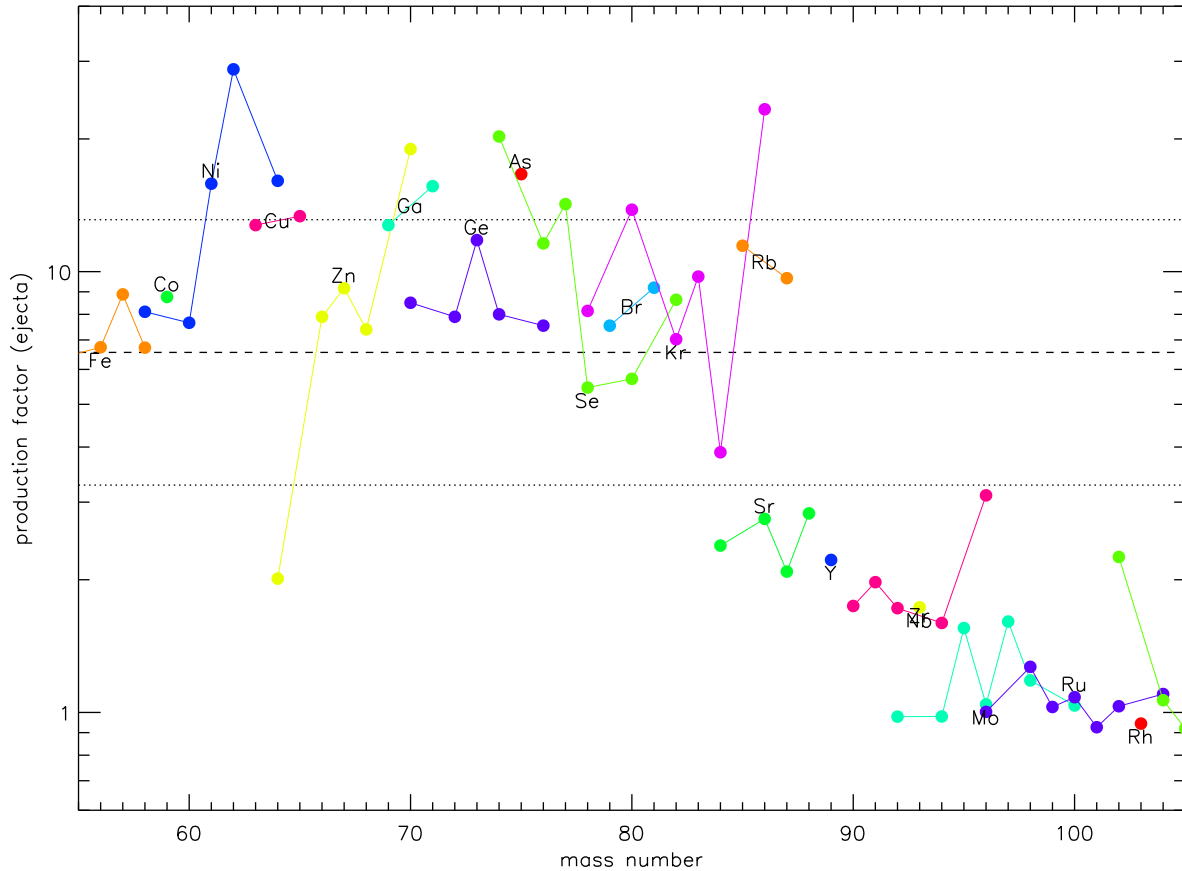


Figure 2: Production factors of trans-iron group nuclei (all isotopes are on scale)

1.3.3 Light Elements and the Iron Group

The species ^2H , ^3He , lithium, beryllium and boron were destroyed in the envelope of the star during central hydrogen burning. However, substantial ^7Li and ^{11}B were recreated by the ν -process during the explosion [34], as was ^{19}F (Fig. 1). ^{17}O was significantly underproduced as a result of the revised reaction rates for $^{17}\text{O}(p, \alpha)^{14}\text{N}$ and $^{17}\text{O}(p, \gamma)^{18}\text{F}$ [11].

The isotopes ^{18}O through ^{38}Ar are in good agreement with solar abundance ratios. ^{40}Ar and ^{40}K are both significantly higher while other potassium isotopes are lower. This signature for the potassium was also found in other stellar models. The under-abundance of ^{44}Ca was caused by the low yield of ^{44}Ti (Table 1) which beta-decays to calcium. The yield of this isotope strongly depends on the location of the final mass cut, i.e., the amount of fall back, and might also be affected by mixing processes during the supernova explosion. The same caveat also applies for other isotopes that mainly originate from regions close to the neutron star, like ^{56}Ni (see contribution of Kifonidis in these proceedings).

1.3.4 The s-Process

The nuclei above the iron group up to about $A = 90$ (Fig. 2) are produced as secondary isotopes by the s-process starting from iron. When considering galactic chemical evolution these yields are to be combined with those of metal-poor stars that contribute correspondingly

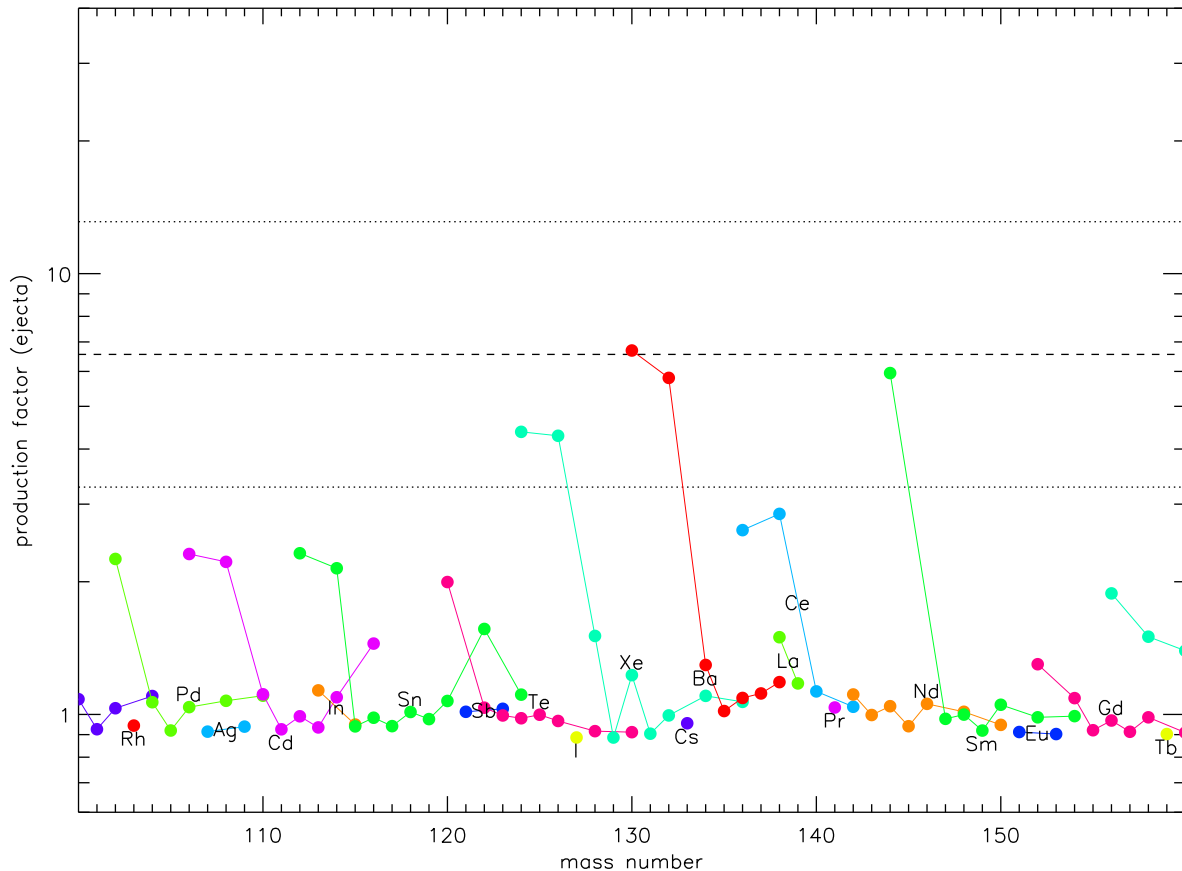


Figure 3: Post iron group nuclei

less of these isotopes, therefore a production factor of about twice that of ^{16}O is in good agreement with reproducing the solar abundance pattern. Note that the yields of these isotopes, by abundance, starting from iron decreases about exponentially. ^{64}Zn , which is underproduced as shown in Fig. 2, may be a product of the neutrino wind from the proto-neutron star [10]. The possible contributions due to this process are not included in the results presented here.

The overabundance of the neutron-rich nickel isotopes, $^{61,62,64}\text{Ni}$, and other s-process products in the $A = 60 - 90$ mass range has been observed before [28, 11] and is still not well understood. It is even greater in stars of 20 and $25 M_{\odot}$. Perhaps the problem will be alleviated by a more complete grid of supernovae of various metallicities and masses, perhaps the stellar structure will be altered by still uncertain physics (overshoot, $^{12}\text{C}(\alpha, \gamma)^{16}\text{O}$, rotation), or perhaps key reaction rates responsible for neutron production or absorption will change. For now, it remains problematic.

Above $A = 100$ (Figs. 3 and 4) the s-process had only minor effects in this $15 M_{\odot}$ star, though there were important “redistributions” of some of the heavy isotopes. Most of the s-process above mass 90 is believed to come from AGB stars.

The “cutoff” towards lower values at a production factor of ~ 0.9 is due to the fact that most of the star does not become hot enough to affect the abundances of these nuclei, or is even lost in the wind. The supernova ejecta containing regions depleted by the s-process and

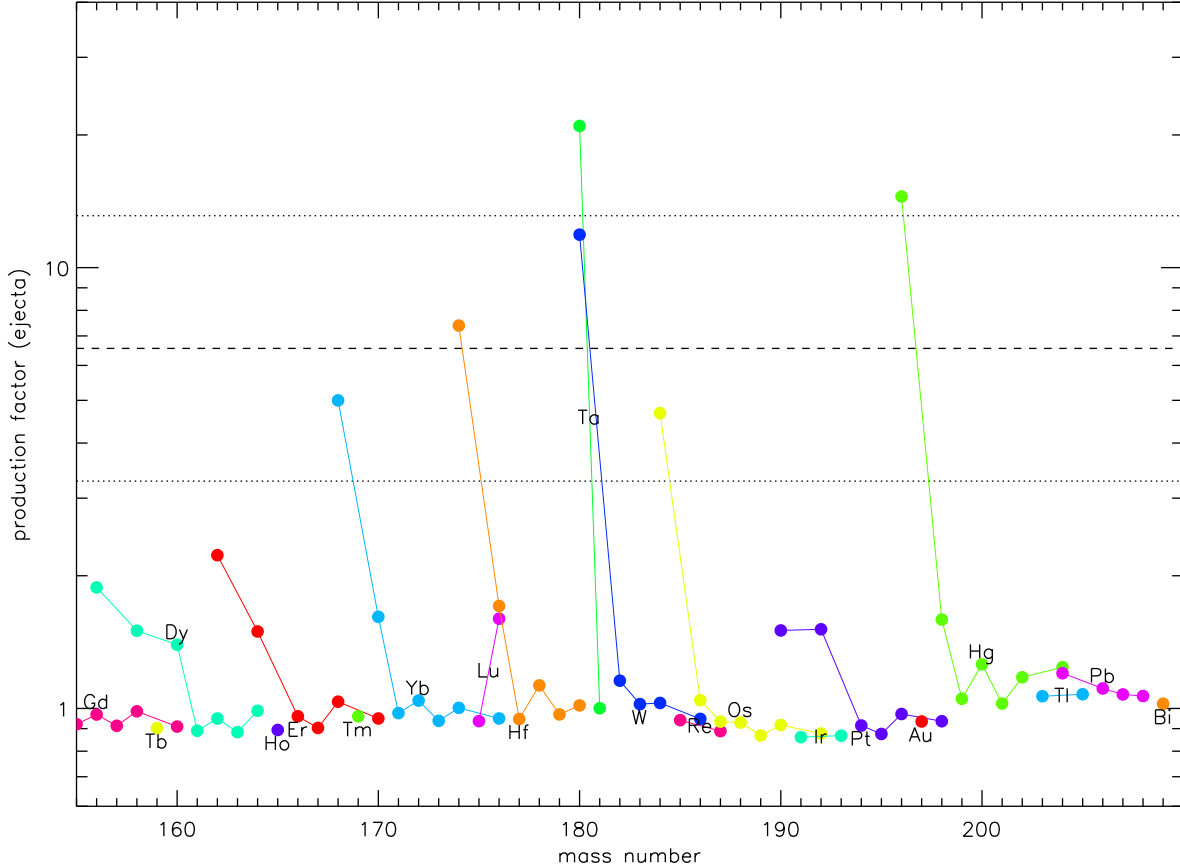


Figure 4: Heavy nuclei

other processes are then averaged with the dominating contribution of unaffected matter. In the $15 M_{\odot}$ star presented here, this leads to the fact that 80% of all *ejecta*, including winds, did not experience the s-process.

1.3.5 The γ -Process

The production of the proton-rich nuclei results from photo-disintegration of heavy nuclei during implosive and explosive oxygen and neon burning (γ -process [30, 23, 24]). Here we present the results of the first calculations that follow the γ -processes through the presupernova stages and the supernova explosion in the whole star. Fully self-consistent, the γ -process here operates in stellar regions that were exposed to previous episodes of s-processing.

Above $A = 123$ to $A = 150$ and between $A = 172$ and $A = 200$ the proton-rich heavy isotopes are produced in solar abundance ratios within about a factor of two relative to ^{16}O (Figs. 3 and 4). Below $A = 123$ and around $A = 160$ the production of the proton-rich isotopes is down by about a factor of three to four. The total production of the proton-rich isotopes increases for higher entropy in the oxygen shell, i.e., with increasing mass of the helium core, as we have seen in our $25 M_{\odot}$ star, but also depends on details of stellar structure and the composition of the star at the time of core collapse. Therefore the contribution from more massive stars may well fill in the gaps of the low production factors seen in the $15 M_{\odot}$ star.

The isotope ^{180}Ta , the rarest stable nuclear species in the solar abundance pattern, shows

a remarkable overproduction (Table 4) in all of our models, despite our taking into account its destruction by de-excitation into the short-lived ground state through thermal excitation into an intermediate state [2]. This may indicate that decay from other excited states could be important, which are not accounted for here. We cannot exclude, however, that our treatment of ^{180}Ta as a single species in the excited state only may cause, at least in part, the overproduction found here.

1.3.6 The r- and n-Process

The base of the helium shell is suspected to be a possible site for fast neutron capture processes as the supernova shock front passes these layers, especially in the less massive core collapse supernovae. Since current models of r-process sites have difficulties in reproducing the r-process peak around $A = 130$ when adjusted to fit the heavier nuclei (see the contribution of Truran in these proceedings), the base of the helium shell was considered as a possible environment for producing these isotopes.

In our present models a distinct redistribution of nuclei around $A = 123$ was found at the base of the helium shell, but the resulting yields were too small to constitute a significant contribution that would be visible in Fig. 3. We may speculate that less massive core collapse supernovae might have a stronger contribution though. More details on the present calculations will be given in [22].

1.4 Conclusions

We have presented the first calculation to follow the complete s-process through all phases of stellar evolution and the γ -process in the whole star through the presupernova stage and subsequent supernova explosion. Below, we summarize the important results for our $15M_{\odot}$ star. Note, however, that though this mass is a numerically typical case of a Type II or Ib supernova, the average nucleosynthetic yield of massive stars is the result of populations of different stars each of which has its own peculiar yields which must be combined to result in a solar-like abundance pattern. Some isotopes that are underproduced here may be strongly overproduced in other massive stars while isotopes overproduced here may be deficient in others.

The proton-rich heavy isotopes above $A = 123$ can be well produced by the γ -process occurring during implosive and explosive oxygen and neon burning. The proton-rich isotopes around $A = 160$ and those between $A = 100$ and $A = 123$, however, are underproduced by a factor of 3 to 4 with respect to ^{16}O . The isotope ^{180}Ta shows a strong overproduction by the γ -process. This may indicate that decay from excited states, of which we include only one, could be important.

A strong secondary s-process contribution appears between iron and a mass number of $A = 90$. Above $A = 100$ the s-process in our $15M_{\odot}$ star is very weak, but it becomes notably stronger in stars with more massive helium cores that perform helium burning at higher entropies.

The expected r- or n-process contribution due to the supernova shock front running through the base of the helium shell does not show a significant contribution in any of our preliminary model stars, not even at $A = 130$. We observed some redistribution of isotopes at the base of helium shell around $A = 123$, but this did not show the characteristics of a typical r-process nor was it important compared to the total yield of the star.

The revisions of opacity tables and the introduction of mass loss generally leads to smaller helium core sizes which tend to also decrease the mass of the carbon-oxygen and the silicon core (Table 1). Note, however, that the absolute values of these core masses depend on the uncertainties, in particular, of the mixing processes in the stellar interior, such as semiconvection, overshooting, and rotation.

The revision of the weak rates [16], important after central oxygen burning, leads to a 2–3% higher electron fraction per nucleon, Y_e , at the time of core collapse in the center of the star (Table 1) and the “deleptonized core” tends to comprise less mass [8]. More important for the core collapse supernova mechanism might be the 30 – 50% higher densities of the new models between the region of $m = 1.5 - 2 M_\odot$ [8], which may result in a correspondingly higher ram-pressure of the infalling matter.

Acknowledgements

We thank Karlheinz Langanke and Gabriel Martínez-Pinedo for discussion and supplying their theoretical weak reaction rates [16] and are grateful to Frank Timmes for providing us with his implementation of the neutrino loss rates of [13] and the sparse matrix inverter we used for the large network. This research was supported, in part, by Prime Contract No. W-7405-ENG-48 between The Regents of the University of California and the United States Department of Energy, the National Science Foundation (AST 97-31569, INT-9726315), and the Alexander von Humboldt-Stiftung (FLF-1065004). T.R. acknowledges support by a PROFIL professorship from the Swiss National Science foundation (grant 2124-055832.98).

References

- [1] Z.Y. Bao, H. Beer, F. Käppeler, F. Voss, K. Wisshak, and T. Rauscher, *ADNDT* **76** (2000) 1.
- [2] D. Belic, et al., *Phys. Rev. Lett.* **83** (1999) 5242.
- [3] J.B. Blake, S.E. Woosley, T.A. Weaver, and D.N. Schramm, *ApJ* **248** (1981) 315.
- [4] J.J. Cowan, A.G.W. Cameron, and J.W. Truran, *ApJ* **294** (1985) 656.
- [5] C. Freiburghaus, et al., *ApJ* **516** (1999) 381.
- [6] Zs. Fülöp, et al., *Z. Phys. A* **355** (1996) 203.
- [7] N. Grevesse and A. Noels, in *Origin and Evolution of the Elements*, ed. N. Prantzos, E. Vangioni-Flam, M. Casse, Cambridge, Cambridge Univ. Press (1993) p. 13.
- [8] A. Heger, S.E. Woosley, G. Martínez-Pinedo, and K. Langanke, *ApJ* (2000) in prep.
- [9] A. Heger, S.E. Woosley, R.D. Hoffman, and T. Rauscher, *ApJS* (2001) in prep.
- [10] R.D. Hoffman, S.E. Woosley, G. Fuller, and B.S. Meyer, *ApJ* **460** (1996) 478.
- [11] R.D. Hoffman, S.E. Woosley, and T.A. Weaver, *ApJ* (2000) in prep.
- [12] C.A. Iglesias and F.J. Rogers, *ApJ* **464** (1996) 943.

- [13] N. Itoh, H. Hayashi, A. Nishikawa, and Y. Kohyama, *ApJS* **102** (1996) 411.
- [14] K.L. Kratz, et al., priv. com. (1996).
- [15] K.L. Kratz, et al., *ApJ* **402** (1993) 216.
- [16] K. Langanke and G. Martínez-Pinedo, *Nucl. Phys.* **A673** (2000) 481.
- [17] P. Möller, J.R. Nix, W.D. Myers, and W.J. Swiatecki, *ADNDT* **59** (1995) 185.
- [18] P. Möller, J.R. Nix, and K.L. Kratz, *ADNDT* **66** (1997) 131.
- [19] H. Nieuwenhuijzen and C. de Jager, *A&A* **231** (1990) 134.
- [20] J.K. Tuli, et al., *Nuclear Wallet Charts*, 5th edition, Brookhaven National Laboratory, USA (1995).
- [21] T. Rauscher and F.-K. Thielemann, *ADNDT* **75** (No. 1+2) (2000) 1.
- [22] T. Rauscher, R.D. Hoffman, A. Heger, and S.E. Woosley, *ApJ* (2000) in prep.
- [23] M. Rayet and M. Arnould, and N. Prantzos, *A&A* **227** (1990) 517.
- [24] M. Rayet, M. Arnould, M. Hashimoto, N. Prantzos, and K. Nomoto, *A&A* **298** (1995) 517.
- [25] E. Somorjai, et al., *A&A* **333** (1998) 1112.
- [26] F.-K. Thielemann, priv. com. (1992).
- [27] F.-K. Thielemann, K. Nomoto, and M.-A. Hashimoto, *ApJ*, **460** (1996) 408.
- [28] F.X. Timmes, S.E. Woosley, T.A. Weaver, and S.E. Woosley, G. Fuller, and B.S. Meyer, *ApJS* **98** (1995) 617.
- [29] A. Weiss, priv. com. (1996).
- [30] S.E. Woosley and W.M. Howard, *ApJS* **36** (1978) 285.
- [31] Woosley, S. E., Wilson, J. R., Mathews, G., Meyer, B., and Hoffman, R. D., *ApJ*, **433** (1994) 229.
- [32] S.E. Woosley and T.A. Weaver, *ApJS* **101** (1995) 181.
- [33] T.A. Weaver, G.B. Zimmermann, and S.E. Woosley, *ApJ* **225** (1978) 1021.
- [34] S.E. Woosley, R.D. Hoffman, D. Hartmann, and W. Haxton, *ApJ* **356** (1990) 272.